Journal of Molecular Structure 1231 (2021) 129895

Contents lists available at ScienceDirect

Journal of Molecular Structure

journal homepage: www.elsevier.com/locate/molstr

Corrosion inhibition performance of a structurally well-defined 1,2,3-triazole derivative on mild steel-hydrochloric acid interface

Meryem Hrimla[a], Lahoucine Bahsis[a,b], Aziz Boutouil[a], My Rachid Laamari[a,*], Miguel Julve[c], Salah-Eddine Stiriba[a,c,*]

[a] Laboratoire de Chimie Analytique et Moléculaire /LCAM, Université Cadi Ayyad, Faculté Polydisciplinaire de Safi, Sidi Bouzid. B.P. 4162, 46 000 Safi, Morocco
[b] Département de Chimie, Faculté des Sciences d'El Jadida, Université Chouaïb Doukkali, B.P.:20, El Jadida 24000, Morocco
[c] Instituto de Ciencia Molecular/ICMol, Universidad de Valencia, C/Catedrático José Beltrán 2, 46980, Valencia, Spain

ARTICLE INFO

Article history:
Received 17 August 2020
Revised 28 December 2020
Accepted 29 December 2020
Available online 17 January 2021

Keywords:
1,2,3-Triazole
Click chemistry
Mild steel
Acidic medium
Adsorption
Corrosion
DFT calculations

ABSTRACT

In the present work, a new 1,4-disubstituted-1,2,3-triazole product, named 4-[1-(4-methoxy-phenyl)-1*H*-[1,2,3]triazol-4-ylmethyl]-morpholine (**MPTM**) was successfully synthesized under click chemistry regime. The structure of the new compound that has a rigid triazole moiety and a flexible morpholine ligand has been characterized using ^{1}H NMR, ^{13}C NMR, HRMS, and FTIR spectroscopy. Its inhibition performance for mild steel in acidic medium 1 M HCl has been studied by utilizing a combination of experimental, spectroscopic and computational methods. The electrochemical characterization was carried out by a gravimetric study, electrochemical impedance spectroscopy (EIS), and potentiodynamic polarization (PDP) measurements. The **MPTM** exhibits a high corrosion inhibition efficiency of 94% with 900 ppm at 298 K. Adsorption of **MPTM** on the mild steel surface followed the Langmuir isotherm. Data obtained from the surface analysis by scanning electron microscopy (SEM), energy dispersive X-ray (EDX), and FTIR spectroscopies evidenced the dual chem- and physi-adsorption of the inhibitor 1,2,3-triazole derivative on the surface of the metal. A quantum chemistry study was performed by means of density functional theory (DFT) to rationalise the adsorption of **MPTM** and its corrosion inhibition action at the interface of mild steel-hydrochloric acid system, establishing a very good correlation between the molecular structure and its inhibition property.

1. Introduction

1,2,3-triazoles are *N*-heterocyclic compounds containing a five-member ring with three nitrogen atoms. Their derivatives are used in a wide variety of applications ranging from biology and pharmaceuticals to the development of large quantities employed as corrosion inhibitors [1-3] leading to minimize the corrosion process in metals and alloys, which is a serious problem worldwide [4-6]. The use of these additives constitutes a significant progress because of their economical synthetic routes and their high inhibitory efficiency [7,8]. Further research has confirmed that organic molecules containing electron-donors such as oxygen (O), nitrogen (N), sulphur (S) atoms and conjugated groups, can act as powerful inhibitors for the prevention of corrosion of metals by acids [9-11]. These heteroatoms can form a coordinative bond by directing their electron pairs towards the 3d orbitals of the iron atom [12-16]. Generally, the adsorption capacity of corrosion-inhibiting particles on the metal surface is based on the three following points: (*i*) the quality and surface condition of the metal component, (*ii*) the type of corrosive environment, and (*iii*) the chemical composition of the corrosion inhibitors.

We herein report the inhibition performance of the new flexible multidentate 1,2,3-triazole compound, namely 4-[1-(4-methoxy-phenyl)-1*H*-[1,2,3]triazol-4-ylmethyl]-morpholine (here after noted **MPTM**), synthesized under click chemistry strategy by using the copper-catalyzed azide-alkyne cycloaddition (CuAAC) reaction [17–19]. Triazole compounds have attracted the attention of a lot of research due to their bioactivity, molecular recognition, and potential applicability to surfactants [20-22]. **MPTM** has been fully characterized using NMR, High Resolution Mass Spectrometry (HRMS), Infra-Red (FTIR) and and UV–Vis spectroscopies, and elemental analysis. Its inhibitory effect was investigated by using electrochemical impedance spectroscopy (EIS) and potentiodynamic polarization (PDP) tests. The presence of a protective layer on the surface of the mild steel (MS) was confirmed by scanning electron miscroscopy (SEM) analyses. Furthermore, in the order to account

* Corresponding authors.
E-mail addresses: r.laamari@gmail.com (M.R. Laamari), stiriba@uv.es (S.-E. Stiriba).

https://doi.org/10.1016/j.molstruc.2021.129895
0022-2860/

for the adsorption phenomenon of **MPTM**, the adsorption models of the title compound were tested during the corrosion prevention process by using Freundlich, Langmuir, and Temkin methodologies [23,24]. Theoretical studies were employed to rationalize the adsorption mechanism of the **MPTM** compound over the mild steel surface.

2. Experimental section

2.1. Materials and Methods

Morpholine, propargyl bromide, triethylamine, sodium azide and 4-methoxyphenylamine were purchased from Sigma-Aldrich and used as received. Anhydrous magnesium sulphate was used to dry the organic extracts, and all volatile substances were removed under reduced pressure. The reaction mixtures were monitored by Thin Liquid Chromatography (TLC), using commercial glass backed TLC plates (Merck Kieselgel60 F254). Revelation was done under an ultraviolet lamp at 254 nm and the melting point was determined using an Electrothermal 9100.

The nuclear magnetic resonance spectra of the proton (^{1}H NMR, 300 MHz) and carbon (^{13}C NMR, 75 MHz) were recorded in deuterated chloroform ($CDCl_3$) on a Bruker Advance DPX 300 device at room temperature with TMS as an internal standard. HRMS were performed on a Varian MAT 311 (EI) or a high-resolution MS/MS ZabSpec TOF Micromass (ESI). FTIR spectra were carried out on an FTIR Nicolet 5700 spectrometer (4000-400 cm^{-1}). The UV-Vis spectra were done with a UV-6300 PC Double Beam spectrophotometer (200 to 800 nm). The SEM analyses of MS were performed employing Field Emission Scanning Electron Microscopy (FESEM) (VEGA3 TESCAN) previously and post-exposure to a hydrochloric medium (1 M) in the absence and presence of the optimal concentration of inhibitor for 24 h at 298 K. The accelerator beam energy applied was 20 kV.

2.2. Synthesis of the 1,2,3-triazole compound

2.2.1. Synthesis of 1-azido-4-methoxybenzene

4-Methoxyphenylamine (13 mmol) was suspended in 80 mL of hydrochloric acid (17%) at room temperature, and then ethanol was added until a clear solution was obtained. The solution was cooled to 0 °C, and small portions (1.5 eq) of $NaNO_2$ were added. 1.5 eq of NaN_3 was slowly added after stirring for 15 minutes at 0 °C. The mixture was kept under stirring for 2 hours at room temperature. The reaction mixture was extracted with diethyl ether (3 × 80 mL). The organic phase obtained was washed with a saturated solution of $NaHCO_3$ and NaCl (50 mL). After drying with anhydrous $MgSO_4$, the organic solvent was removed under reduced pressure, and the desired 1-azido-4-methoxybenzene (**1**) was obtained as a brown liquid without any further purification.^{1}H NMR (300 MHz, $CDCl_3$): δ (ppm) = 6.95 - 6.90 (m, 2H, CH), 6.88 - 6.83 (m, 2H, CH), 3.76 (s, 3H, OMe) [25,26].

2.2.2. Synthesis of 4-[1-(4-methoxy-phenyl)-1H-[1,2,3]triazol-4-ylmethyl]-morpholine (*MPTM*)

The reaction was carried out in two steps:(*i*) the nucleophilic substitution reaction between morpholine and propargyl bromide, and (*ii*) the CuAAC reaction between the obtained terminal alkyne and azide. Initially, the nucleophilic substitution reaction was performed as follows: a mixture of water (5 mL), Et_3N (1.5 mmol), organic amine (morpholine) (0.5 mmol) and propargyl bromide (0.5 mmol) was stirred for 10 minutes at 80 °C. Then, $Cu(OAc)_2$ (5 mol%) and ascorbic acid (5 mol%) were added and the reaction mixture was stirred at 80 °C for 4h. After compilation, the reaction mixture was cooled to room temperature and $Cu(OAc)_2$ was removed by simple filtration. The product was extracted with ethyl acetate (3 × 10 mL). The combined organic extracts were washed with saturated NaCl and dried with anhydrous $MgSO_4$. After removal of the organic solvent under reduced pressure, the residue was purified by flash chromatography on silica gel using ethyl acetate as an eluent to afford the desired product (Table 1).

The product was obtained as a brown solid. Yield: 89%. Mp: 100-102 °C. FTIR (KBr) ν/cm^{-1}: 3423.10, 3142, 1520.45 (N-H stretch); 3023.66, 905.90 (=CH stretch); 2929.75, 2801.51, 1448.47 (CH_3 stretch); 1610.60 (C=C stretch); 1116.50, 1034.69 (C-O stretch); 1314.16, 1216.25 (C-N stretch). ^{1}H-NMR ($CDCl_3$, 300 MHz, δ (ppm)) 2.51 (dd, J = 5.0, 3.5 Hz, 4H), 3.66 (dd, J= 5, 3.4 Hz, 4H), 3.68 (s, 3H, CH_3), 3.80 (s, 2H, CH_2), 6.95 (d, J = 9.1 Hz, 2H, CH_2), 7.56 (d, J = 9.1 Hz, 2H, CH_2), 7.79 (s, 1H, $CH_{triazole}$). ^{13}C-NMR [$CDCl_3$, 75 MHz, δ (ppm)], 53.4 (2 CH_2), 53.6 (CH_2), 55.6 (CH_3), 66.8 (2 CH_2), 114.8 (2 HC_{ar}), 121 ($HC_{triazole}$), 122 (2 HC_{ar}), 130.5 (C_q), 144.6 (C_q), 159.9 (C_q). HRMS (FAB+) *m/z*: Calcd for $C_{14}H_{18}N_4O_2$: 275.1503 Found: 275.1511. (Figs. S1 and S2 in Supporting Information).

2.3. Corrosion Inhibition Study

2.3.1. Materials Preparation

The MS sample having the following chemical composition (wt %): O (0.03); Mn (0.048); N (0.012); S (0.012); C (0.016); P (0.001) and the balance was Fe was used to carry out the corrosion inhibition experiments. MS was cleaned with double distilled water, degreased with acetone, washed again with doubly distilled water, soaked in acetone and alcohol, and dried at room temperature. All potential measurements in the experimental studies refer to the saturated calomel electrode (SCE), and the counter electrode is a platinum plate with a surface area of 2 cm^2. The corrosive medium tested was prepared with an analytical quality of HCl (37% by weight), and deionized water. The concentration of **MPTM** used was changed from 300 to 900 ppm.

2.3.2. Gravimetric Measurements

Gravimetric measurements were carried out in a double-walled glass cell fitted with a thermostat-cooled condenser. The steel samples employed (2 × 2 × 0.05 cm^3) were carefully cleaned with double distilled water, degreased with acetone, washed again with doubly distilled water, soaked in acetone and alcohol, dried, and then weighed by using an electronic scale. Subsequently, they have been drenched in 1 M HCl solution with and without different concentrations of **MPTM** for 6 h at various temperatures (from 298 to 328 K), separately. Experimental tests were conducted in each case, and the average weight loss was considered to estimate the corrosion rate in mg cm^{-2} h^{-1} and the inhibition efficiency (IE_W%) according to the following equation:

$$IE_w\ (\%) = \frac{C_{R_o} - C_R}{C_{R_o}} \times 100 \qquad (1)$$

where C_{Ro} and C_R are the corrosion rates in the lack and presence of the inhibitor, respectively.

2.3.3. Electrochemical Methods

The electrochemical measurements were carried out using the Voltalab 10 system (PGZ 100 radiometer) controlled by the corrosion analysis software Volta master 4. Firstly, the open circuit potential (OCP) was determined by the immersion of the electrodes in 1 M HCl for an hour, with and without the addition of inhibitor. The impedance tests were executed in the interval of 100 kHz to 0.1 Hz, with an amplitude of 10 mV, using the AC signal at E_{ocp}. The electrochemical impedance parameters were obtained using EC-Lab software Bio-Logic Science Instruments, Seyssinet-Pariset, France. Next, the potentiodynamic polarization curves were carried

Table 1
Structure and data of **MPTM**

	Name	Structure	MW (g/mol)	Formula	Mp(°C)
MPTM	4-[1-(4-Methoxy-phenyl)-1*H*-[1,2,3]triazol-4-ylmethyl]-morpholine	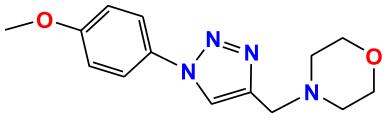	274.1503	$C_{14}H_{18}N_4O_2$	100-102

out in a potential range of -800 to -300 mV/SCE. The inhibitor effectiveness was calculated for the EIS and PDP tests according to equations (2) and (3), respectively [27]:

$$IE\% = \frac{R_{pi} - R_p}{R_{pi}} \times 100 \quad (2)$$

$$IE\% = \frac{I - I_i}{I} \times 100 \quad (3)$$

where R_{pi} and R_p (R_p=R_{ct}+R_f) stand for the values of the polarization resistance in the presence and absence of inhibitor I and I_i represent the density of the corrosion current in the absence and the presence of inhibitor, respectively.

2.4. Surface analysis

2.4.1. UV-Visible Spectroscopy

Spectrophotometric UV-Vis absorption measurements were performed in a solution containing an optimal concentration (900 ppm) of **MPTM** inhibitor before and after immersion of the MS sample for 3 days at 298 K. All spectra were recorded using a UV-6300 PC Double Beam Spectrophotometer (200-800 nm) operating at 1 nm resolution with a scanning rate of 100 nm min^{-1} at room temperature.

2.4.2. FTIR Spectroscopy

MS surfaces are immersed for 24 h in the acidic medium (1 M HCl) before and after the addition of the inhibitor (900 ppm). The FTIR spectrum of the protected film was recorded using the Nicolet 5700 spectrometer to detect the presence of the **MPTM** inhibitor.

2.4.3. SEM Surface

Cleaned MS samples by the previously announced method were immersed in 1 M HCl in the absence and presence of an optimal concentration (900 ppm) of **MPTM** after 24 h at room temperature. Then, their elementary information was analyzed by SEM using the VEGA3 TESCAN model equipped with an energy dispersive X-ray analysis (EDX).

2.5. Quantum Chemical (QC) Calculations

The optimized geometry of the **MPTM** molecule was performed using Density functional theory (DFT) calculations at B3LYP/6-31G(d,p) level on the Gaussian 09 software package [28]. The vibrational analysis was carried out to confirm that the optimized geometry of **MPTM** is the minimum point on the potential energy surface. Both the highest occupied molecular orbital (HOMO) and lowest unoccupied one (LUMO) and the MEP of the studied molecule are computed at the same theoretical level. Further, the Fukui functions are calculated based on the two expressions given hereunder [29]:

$$f_k^- = [q_k(N) - q_k(N-1)]\ for\ electrophilic\ attacks \quad (4)$$

$$f_k^+ = [q_k(N+1) - q_k(N)]\ fornucleophilicattacks \quad (5)$$

Table 2
Corrosion parameters obtained from the weight loss measurements for steel in 1 M HCl containing various concentrations of **MPTM** at 298 K.

	C_{inh} (ppm)	CR (mg cm^{-2} h^{-1})	θ	IE_w (%)
Blank	1(**M**)	0.3857	-	-
MPTM	300	0.0605	0.8431	84.31
	500	0.0422	0.8905	89.05
	700	0.0306	0.9206	92.06
	900	0.0231	0.9401	94.01

where $q(N)$, $q(N+1)$ and $q(N-1)$ are the charges at atom k on the neutral, anionic, and cationic species, respectively. The dual descriptor was performed using Multiwfn [30] in order to illustrate the most electrophilic and nucleophilic sites in the **MPTM** molecule, and defined as:

$$Df_k(r) = f_k^+ - f_k^- \quad (6)$$

where $\Delta f_k > 0$ and $\Delta f_k < 0$ stand for the electron acceptor and electron donate sites, respectively.

3. Results and Discussion

3.1. Synthesis of 1,2,3-triazole compound (MPTM)

The synthetic reaction used for the preparation of the new 1,2,3-triazole compound, namely 4-[1-(4-methoxyphenyl)-1*H*-[1,2,3]triazol-4-ylmethyl]-morpholine **MPTM** is illustrated in **Scheme 1**. **MPTM** was obtained under copper catalyzed alkyne-azide cycloaddition reaction, in a regioselective manner as 1,4-disubstituted 1,2,3-triazole by three-components cycloaddition reaction of morpholine, propargyl bromide with azido-4-methoxybenzene (**1**) using $Cu(OAc)_2$ as catalyst and Et_3N as a base in water as solvent (Scheme 1). The desired triazole product **MPTM** was isolated as a brown solid with a yield of 89%. The prepared triazole was characterized by FTIR, NMR, HRMS and elemental analyses confirming the molecular structure of **MPTM**. It deserves mentioning that the new 1,2,3-triazole bearing morpholine moiety **MPTM** has a triazole unit, π-electrons aromatic group and morpholine pendent moiety, which may lead to an organic compound with potential corrosion inhibiting features.

3.2. Gravimetric Measurements

The data obtained from weight loss measurements for MS in 1 M HCl solution without and with several concentrations of **MPTM** are presented in Table 2, Figs. 1 and 2. As one can see in Table 2, the corrosion inhibition efficiency of the inhibitor improves with the concentration. This reveals that **MPTM** effectively acts as a corrosion inhibitor, with an inhibition efficiency of 94.01% at 900 ppm. Fig. 1 shows the plot of the inhibition efficiency *vs.* the concentration of the inhibitor at the different temperatures. Examination of the plots reveals that the corrosion inhibition efficiency IE_w(%) increases with the increase in the concentration of **MPTM** from 300 to 900 ppm, and it decreases with an increase of the temperature. Significant corrosion inhibition efficiency was

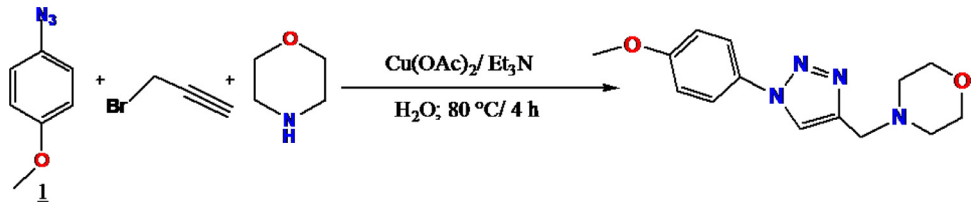

Scheme 1. Synthetic scheme of **MPTM**.

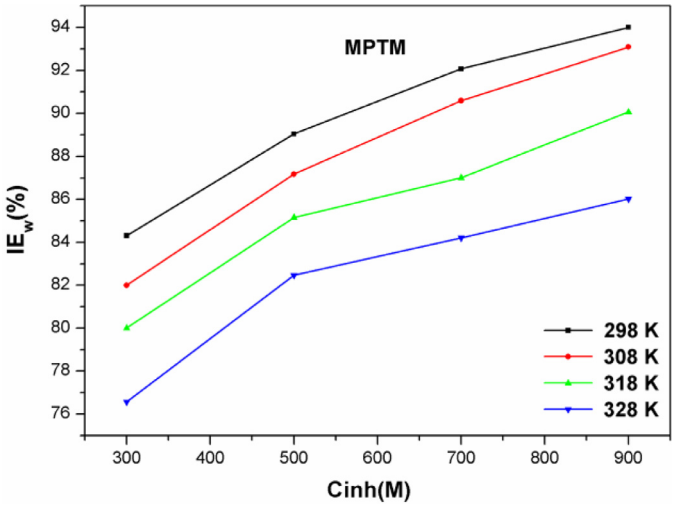

Fig. 1. Variation of the inhibition efficiency with diverse concentrations of **MPTM** in 1 M HCl solution at various temperatures.

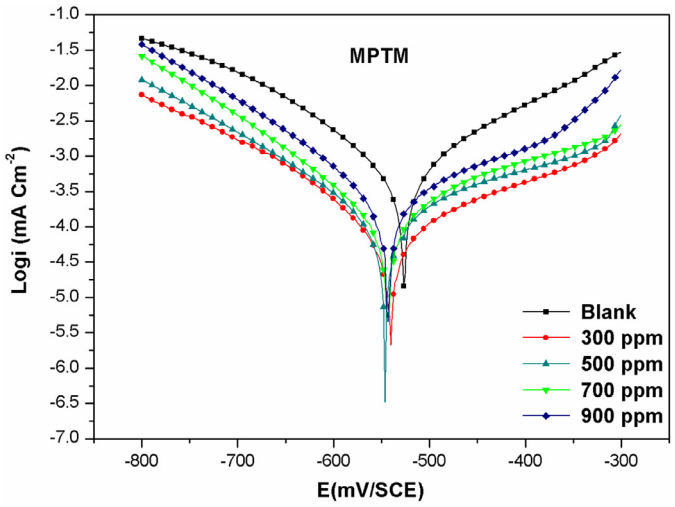

Fig. 3. PDP curves for MS in the lack and presence of various concentrations of **MPTM** at 298 K.

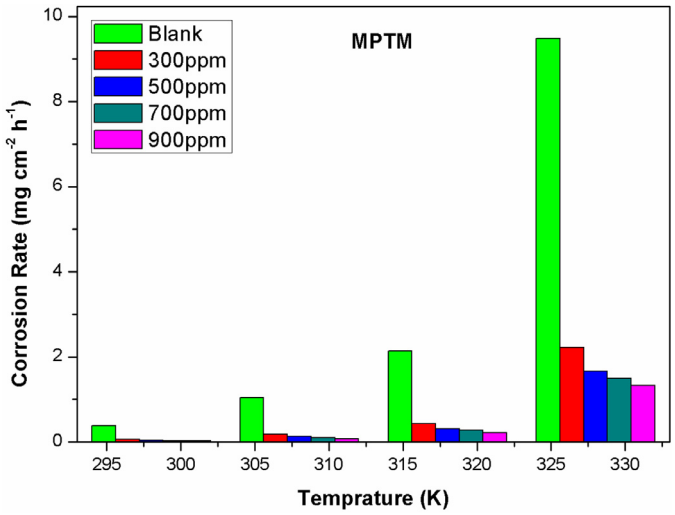

Fig. 2. Impact of the **MPTM** concentration on the corrosion rate at different temperatures.

observed even at low concentrations of **MPTM** (Table 2). This indicates its capacity as an effective inhibitor. Fig. 2 represents the plot of the corrosion rate (CR) of MS against the concentrations at different temperatures. The CR increases with the increasing of the temperature whereas it decreases with an increase of the **MPTM** concentration. That can be interpreted in terms of a metal dissolution process being enhanced while the rate of desorption of the inhibitor molecule is larger at higher temperatures [31,32].

3.3. Effect of the inhibitor concentration

3.3.1. PDP Study

Potentiodynamic polarization tests have undertaken to distinguish the effect of **MPTM** on the anodic dissolution of MS and cathodic hydrogen ion reduction. Fig. 3 shows the PDP curves for MS in 1 M HCl solution before and after the addition of the various concentrations of **MPTM** at 298 K. The corrosion parameters such as corrosion potential (E_{corr}), cathodic Tafel slope (βc), anodic Tafel slope (βa), and corrosion current density (i_{corr}), as well as inhibitory efficacy ($\%IE$) obtained from these curves, are listed in Table 3. Each increase in the **MPTM** inhibitor concentration results into smaller current densities for both the anodic and the cathodic branches of the PDP curves. However, Tafel's cathodic and anodic slopes and the corrosion potential are practically unchanged. Furthermore, an inspection of the polarization curves illustrated by Fig. 3 indicates that the cathodic and anodic curves have shifted towards the side of lower current density with an increase in the inhibitor concentration. Furthermore, the parallel curves of the cathodic Tafel suggest that the adsorbed inhibitory molecule only blocks the active sites of hydrogen evolution on the metallic surface, thereby making the process of hydrogen evolution unchanged and that the reduction of hydrogen ions on the surface of the mild steel is mainly achieved by a charge transfer mechanism [33,34]. For the anode domain, the addition of **MPTM** inhibitor results into a decrease in the current densities in the high-potential range. Also noted that for potentials above -400 mV, the inhibitor begins to desorb, a feature which is commonly described as a desorption potential [35–37]. In this case, the desorption rate of the 1,2,3-triazole compound is higher than its adsorption [38,39]. Additionally, the presence of **MPTM** in the corrosive environment did not cause any significant change in the values of E_{corr} , implying that the **MPTM** inhibitor acts as a mixed type inhibitor [40].

Table 3
Polarization parameters and the corresponding inhibition efficiency of corrosion of the MS in 1M HCl containing different concentrations of **MPTM** at 298 K

	C_{inh}(ppm)	E_{corr}(mV/SCE)	i_{corr}(mA cm^{-2})	β_a(mV dec^{-1})	β_c(mVdec^{-1})	IE%
Blank	1M	-531.1	0.3856	93.2	-92.6	-
MPTM	300	-547.8	0.0607	43.4	-39.7	84.25
	500	-548.2	0.0422	45.6	-47.2	89.07
	700	-550.7	0.0306	42.5	-41.3	92.06
	900	-545.2	0.0230	47.3	-46.6	94.03

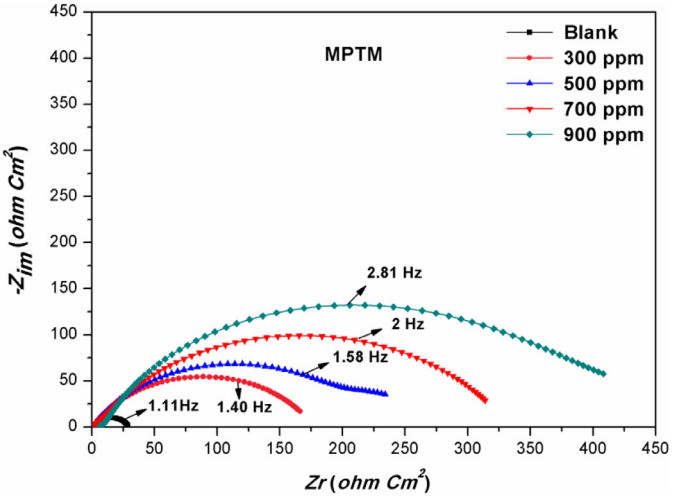

Fig. 4. Nyquist plot for the dissolution of MS in 1 M HCl with and without different concentrations of **MPTM** at 298 K.

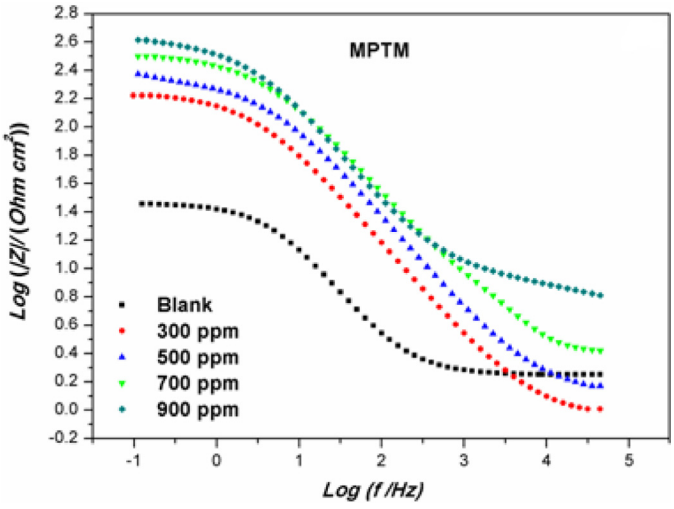

Fig. 5. Bode plots for mild steel in 1 M HCl without and with different concentrations of the **MPTM** inhibitor at 298 K.

3.3.2. Electrochemical Impedance Spectroscopy (EIS)

The corrosion inhibition property of **MPTM** on MS was also examined by another important electrochemical technique. EIS is a non-destructive technique for judging corrosion inhibition performance based on the interaction between the metal and the molecules of inhibitors in an aggressive medium [40]. Figs. 4 and 5 illustrate the Nyquist and Bode plots, respectively, obtained from EIS for mild steel immersed in 1 M HCl solution without and under different concentrations of the **MPTM** inhibitor at 298 K.

The semi-circular form observed in Fig. 4 indicates that the corrosion mechanism remains the same with or without **MPTM** addition [21,40]. However, the diameter of the capacitive loop increases

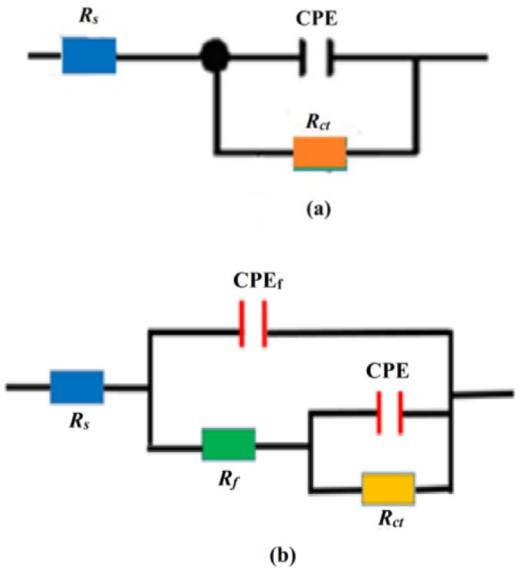

Fig. 6. Equivalent circuits used to adjust the impedance spectra obtained for steel before and after the addition of an **MPTM** inhibitor.

with a further increase in the **MPTM** concentration. Nyquist semicircles undergo frequency dispersion, which is the result of the non-homogeneity or roughness of the metal surface [41]. This phenomenon could be related to the adsorption of the inhibitor on the steel surface. The same behavior can be observed in the Bode diagram Fig. 5). The semi-circular shape did not change after the addition of the **MPTM** inhibitor, which means that the corrosion reaction is under charge transfer control and that the corrosion mechanism has not changed [42]. The equivalent circuits used to fit the impedance parameters in the absence and in presence of different concentrations of **MPTM** inhibitor are trated in (Figs. 6a and 6b), respectively. According to both equivalent circuits, R_s and R_{ct} represent the solution resistance and charge-transfer resistance, respectively. The resistance of the film formed on the metal surface is represented by R_f, Q_f and Q_{dl} stand for the constant phase angle elements constants (CPE), C_f is the reflecting capacitance and C_{dl} accounts for the double-layer capacitance. The impedance function of the CPE and the values of C_{dl}, and C_f are calculated by using the Eqs. (7), ((8), and (9), respectively: [43–45]

$$Z_{CPE} = Y_0^{-1}(j\omega)^{-n} \quad (7)$$

$$C_{dl} = Y_o(\omega_{max})^{n-1} \quad (8)$$

$$C_f = F^2 \,.\, S/4RT \quad (9)$$

In Eq. (7), Y, ω and j represent the CPE constant, the angular frequency and the imaginary number whereas the n coefficient is the phase shift ($-1 \leq n \leq 1$) which demonstrates that CPE could be used as a capacitor (n=1), resistance (n=0), and inductance (n= -1). In Eq. (8), $\omega_{max} = 2\pi f_{max}$, f_{max} being the frequency at which the

Table 4
EIS parameters for the corrosion of MS in the absence and presence of the **MPTM** inhibitor at various concentrations in 1 M HCl at 298 K.

Inhibitor	C (ppm)	R_s(Ω cm^2)	R_f(Ω cm^2)	R_{ct}(Ω cm^2)	R_p(Ω cm^2)	Q_{dl}		Q_f		*IE* (%)
						n_1	C_{dl}(μF cm^{-2})	n_2	C_f(μFcm^{-2})	
MPTM	Blank	1.764	-	27.19	27.19	0.801	113.9	-	-	-
	300	1.484	0.183	170.41	170.6	0.705	87.56	0.993	33.51	84.06
	500	1.266	2.055	245.84	247.9	0.701	82.01	0.936	29.01	89.03
	700	1.591	3.984	340.21	344.2	0.772	73.62	0.999	24.63	92.10
	900	1.631	6.762	446.94	453.7	0.813	66.31	0.803	20.71	94.00

Table 5
Electrochemical parameters and the corresponding corrosion inhibition efficiency of MS without and with different concentrations of the **MPTM** inhibitor at various temperatures.

Temperature (K)	*C* (ppm)	E_{corr}*vs.* SCE (mV)	i_{corr} (mA cm^{-2})	*IE* (%)
298	**Blank**	**-531.1**	**0.3856**	**-**
	300	-547.8	0.0607	84.25
	500	-548.2	0.0422	89.07
	700	-550.7	0.0306	92.06
	900	-545.2	0.0230	94.03
308	**Blank**	**-535.8**	**1.0345**	**-**
	300	-532.7	0.1852	82.09
	500	-540.3	0.1327	87.17
	700	-530.9	0.0973	90.59
	900	-538.7	0.0715	93.10
318	**Blank**	**-545.9**	**2.1351**	**-**
	300	-524	0.4270	80.00
	500	-523	0.3169	85.16
	700	-518.5	0.2774	87.01
	900	-524.6	0.2121	90.01
328	**Blank**	**-542.2**	**9.4741**	**-**
	300	-517.4	2.2208	76.55
	500	-518.2	1.6605	82.47
	700	-512.1	1.4965	84.20
	900	-512.4	1.3235	86.03

imaginary component of the impedance is maximum. Finally, *S* and *F* in Eq. (9) are the surface area of the elecrode exposed to the corrosive solution and the Faraday's constant, respectively.

Table 4 shows the fitted equivalent circuit parameters for mild steel in 1 M HCl with and without the **MPTM** inhibitor at different concentrations at 298K. With the addition of inhibitors, both R_{ct} and R_f values increase as the concentration of **MPTM** increases from 300 to 900 ppm. This phenomenon manifests the formation of inhibitors-adsorption films on the metal surface, leaving fewer electroactive sites available for corrosion [46–50]. This provides a better anti-corrosion efficiency, reaching a maximum value of 94% at 900 ppm. Furthermore, the values of C_{dl} and C_f decrease with the rising of the additive concentration. This can be explained by the decrease of the exposed area of the electrode face by the coverage of the **MPTM** additive on the surface of the working electrode [51].

3.3.3. *Effect of temperature on inhibition efficiency* IE *(%)*

Additional experiments were carried out to check the effect of the temperature on the *IE* using potentiodynamic polarization study (PDP), at various temperatures 298-328 K. According to Fig. 7 and Table 5, it can be seen that I_{corr} increases with increasing the temperature and it is more marked for the uninhibited solution. On the other hand, for each concentration, we observed a slight variation in the inhibition efficiency with the rise of the temperature, which means that the higher temperature does not affect the adsorption of **MPTM** on the surface of the metal. The slightly decreased efficiency of the **MPTM** inhibitor at higher temperatures is due to the shifting of the adsorption-desorption equilibrium towards the desorption [52].

3.4. *Adsorption isotherm*

To get a better understanding of the inhibition mechanism of organic molecules on the surface of the metal and to obtain information on the structural properties, it is necessary to test the adsorption model of **MPTM** during the corrosion inhibition process. In this work, several adsorption isotherms formulae such as Langmuir, Freundlich and Temkin were tested to simulate the link between the inhibitor concentration and the surface coverage such as:

$$\frac{C_{inh}}{\theta} = \frac{1}{K_{ads}} + C_{inh}\ \text{(Langmuir isotherm)} \tag{10}$$

$$\log\theta = n\log C_{inh} + \log K_{ads}\ \text{(Freundlich isotherm)} \tag{11}$$

$$lnC_{inh} = a\theta - \ln K_{ads}\ \text{(Temkin isotherm)} \tag{12}$$

where C_{inh} is the concentration of the inhibitor (which corresponds to the surface coverage obtained from gravimetric measurements), K_{ads} represents the equilibrium constant and the *a* coefficient is the molecular constant (Fig. 8).

Based on the regression coefficient (R^2) and the values listed in Table 6,it can be concluded that the studied compound is adsorbed onto the surface of the MS according to Langmuir isothermal standard. On the other side, the comparatively high K_{ads} values suggest that the compound under examination may be strongly adsorbed on the surface of the metal [53]. The standard free energy of **MPTM** can be determined at different temperatures by the following equation: [54].

$$\Delta G°ads = -RT\ \text{Ln}(55.5Kads) \tag{13}$$

where *R* (in J mol^{-1}K^{-1}) is the universal gas constant, *T* (in K) is the temperature and 55.5 is the molar concentration of water in mol L^{-1}.

As mentioned in the literature, values of free energy around or less than −20 kJ mol^{-1} characterize a physical adsorption process, while the values around or above −40 kJ mol^{-1}, reveal that the adsorption is mainly classified as a chemisorption [55]. In our case, the calculated values of the standard free energy of adsorption cover the range between -61.80 to -31.50 kJ mol^{-1}, suggesting that the adsorption of **MPTM** takes place under both physisorption and chemisorption interactions. Furthermore, the negative values of $\Delta G°_{ads}$ points to the spontaneity of the adsorption process onto the mild steel surface [56,57].

3.5. *Thermodynamic analysis*

3.5.1. *Corrosion kinetic parameters*

To get further details on the corrosion behavior, various corrosion kinetic parameters could be determined using the Arrhenius equation:

$$\log CR = Log\,A - \left(\frac{E_a}{2.303RT}\right) \tag{14}$$

$$log\left(\frac{CR}{T}\right) = \left[\left(Log\left(\frac{R}{Nh}\right)\right) + \left(\frac{\Delta S°}{2.303R}\right)\right] - \frac{\Delta H°}{2.303RT} \tag{15}$$

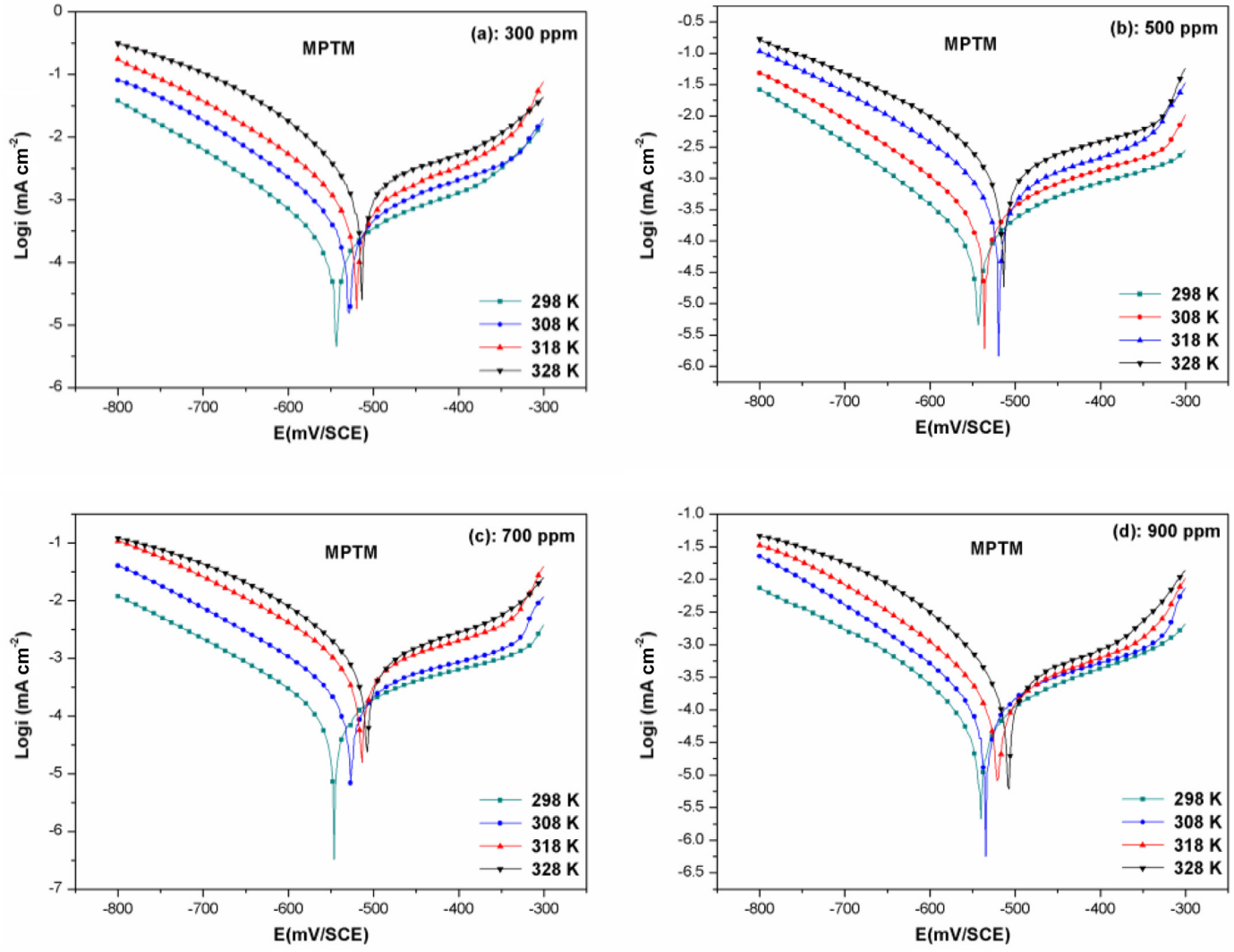

Fig. 7. Tafel plots of MS electrode in 1 M HCl containing different concentrations of **MPTM** at different temperatures.

Table 6
Calculated values of K_{ads} and $\Delta G°_{ads}$ from different adsorption isotherm models of **MPTM** in 1 M HCl at different temperatures.

Inhibitor	Isotherm	T(K)	R^2	K_{ads} (M^{-1})	$-\Delta G°_{ads}$(kJ mol^{-1})	Size and interaction parameters
MPTM	Langmuir	298	0.9998	1.40	61.80	-
		308	0.9996	1.46	53.10	-
		318	0.9992	1.54	41.70	-
		318	0.9998	1.61	31.50	-
	Timken	298	0.9999	1.03	10.01	a = 0.10019
		308	0.9802	1.03	10.34	a = 0.08829
		318	0.9545	1.02	10.68	a = 0.08508
		318	0.9980	1.03	11.03	a = 0.08957
	Freundlich	298	0.9960	0.47	8.10	n = 0.10068
		308	0.9996	0.42	8.10	n = 0.11469
		318	0.9797	0.44	8.46	n = 0.10418
		318	0.9471	0.42	8.61	n = 0.10488

where *CR*, *N*, *R*, *h* and *A* are the corrosion rate, the Avogadro's number, universal gas constant, the Planck's constant and the pre-exponential factor, respectively.

Arrhenius plots for the corrosion rate of MS with and without **MPTM** are given in Figs. 9a and 9b, respectively. The corrosion kinetic parameters, such as the activation energy (E_a), the entropy of activation (ΔS_a°), and enthalpy of activation (ΔH_a°) are shown in Table 7. A plot of log*CR vs.* 1/*T*,gives a straight line having a slope equal to $-E_a/RT$ (Fig. 9a). Another plot of log (CR/T) against 1/*T*, also

Table 7
Activation parameters for mild steel in 1 M HCl in the lack and in the presence of different concentrations of **MPTM**.

C_{inh} (ppm)		E_a (kJ mol^{-1})	$\Delta H_a°$ (kJ mol^{-1})	$-\Delta S_a°$ (kJ mol^{-1} K^{-1})
Blank	1 **M**	87.147	84.5502	51.20
MPTM	300	93.783	89.9166	53.34
	500	95.921	90.5999	53.00
	700	101.632	97.6084	73.60
	900	107.107	105.2687	95.80

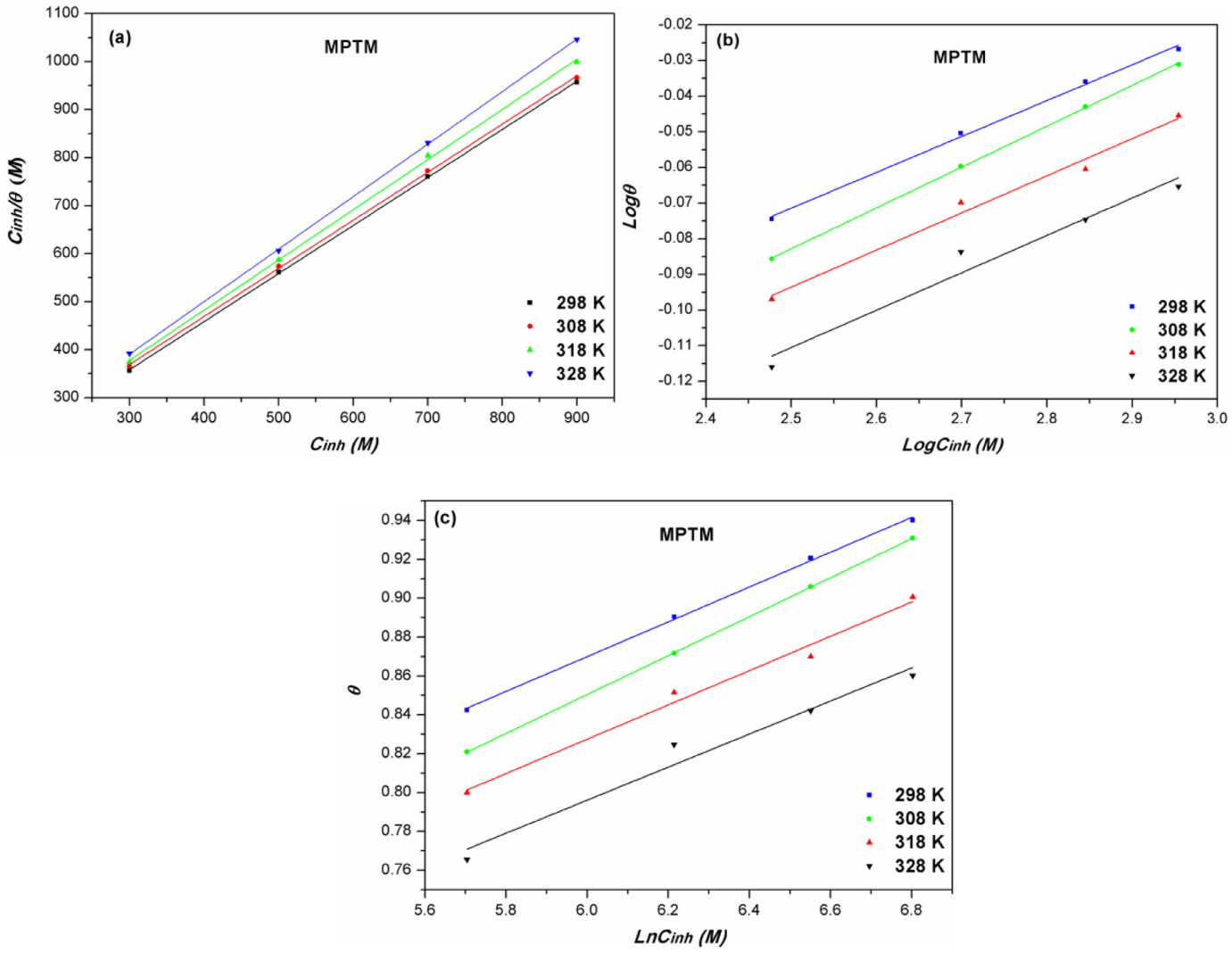

Fig. 8. Thermodynamic Langmuir (a), Freundlich (b) and Temkin (c) adsorption isotherms for MS with different concentrations of **MPTM** at various temperatures after one hour of immersion in 1 M HCl.

gives a straight line with a slope and an intercept which are equal to $-\Delta H^{\circ}/2.303R$ and $\ln(R/Nh) + \Delta S^{\circ}/2.303R$, respectively (Fig. 9b). Table 6 shows that the values of the activation energies increase with increasing the concentration of the inhibitor, a feature which confirms that the addition of **MTPM** could effectively suppress the dissolution of MS [56]. Furthermore, the calculated value of ΔH° is positive, suggesting an endothermic adsorption process, which accounts for the inhibitor's effectiveness at higher temperatures [57]. Moreover, the value of ΔS° is more positive in the inhibited environment than that in the blank solution, a feature that can be attributed to the adsorption of **MPTM** and desorption of water molecules simultaneously during the coverage of inhibitor on the metallic surface [42].

3.5.2. Thermodynamic adsorption parameters

The Van't Hoff equation [Eq (13)] allowed us to determine the different thermodynamic adsorption parameters: the adsorption enthalpy (ΔH°_{ads}) and adsorption entropy (ΔS°_{ads}) using the values of the slope ($\Delta H^{\circ}_{ads}/R$) and the intercept ($-\ln(1/55.5) + \Delta S^{\circ}_{ads}/R$) respectively (Table 8), obtained from the plot of $\ln K_{ads}$ as a function of $1/T$ (Fig. 10).

$$\ln K_{ads} = \ln\frac{1}{55.5} + \frac{\Delta S^{\circ}_{ads}}{R} + \frac{\Delta H^{\circ}_{ads}}{RT} \quad (16)$$

The positive values of ΔH°_{ads} show the endothermic adsorption nature of **MPTM** on the metallic surface [58,59]. Furthermore, the positive values of ΔS°_{ads} are explained by a disorder of the inhibitor molecules adsorbed on the MS surface [60,61].

3.6. UV-Visible spectroscopic study

It has already been reported [62,63] that the corrosion inhibition may result from the formation of a complex involving the metal and the inhibitor molecule. To validate the possibility of the formation of a **MPTM-Fe** complex, the UV-Vis absorption spectra of a 1 M HCl solution containing 900 ppm of **MPTM** before and after 48 hours of immersion of MS samples were performed (Fig. 11). UV-Vis spectra show two characteristic absorption peaks at 205 nm and three peaks at 254-256 and 332 nm. The absorption band peak at 205 nm is associated to the π-π* transitions of the C=C bonds of the aromatic ring [64], while the less intense peaks at 254 and 332 nm correspond to the transition of the n-π* of the N=N groups of the triazole. The results show that after immersion of the steel samples in acidic solutions, the bands at 205 and 256 nm decrease in intensity while the band corresponding to n-π* transition at 332 nm slightly increase. This result point out to the formation of a complex between the Fe^{2+} ion and the **MPTM** inhibitor in acidic medium [65].

Table 8
Adsorption parameters for MS in 1 M HCl in the presence of various concentrations of **MPTM** at various temperatures.

T (K)	lnK_{ads}(M^{-1})	$-\Delta G°_{ads}$(kJ mol^{-1})	$\Delta H°_{ads}$ (kJ mol^{-1})	$\Delta S°_{ads}$ (J mol^{-1} K^{-1})
298	-4.265	61.80	3.66×10^{-3}	10.22
308	-4.223	53.10		
318	-4.174	41.70		
328	-4.131	31.50		

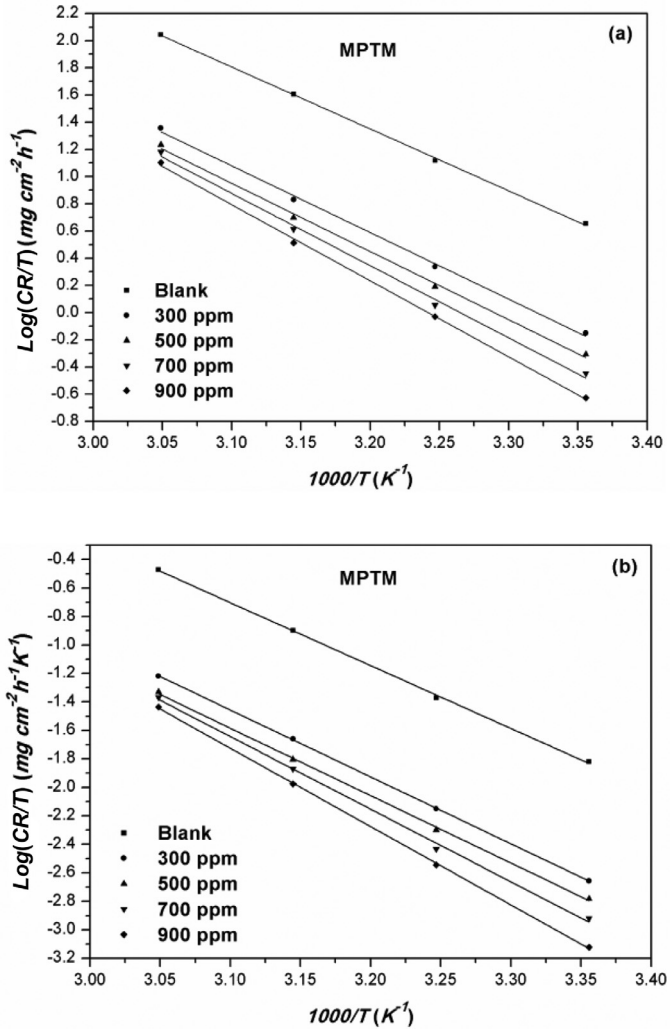

Fig. 9. Thermodynamic curves for MS with various concentrations of **MPTM** after one hour of immersion in 1 M HCl at 298 K: (a) Arrhenius and (b) transition state plots.

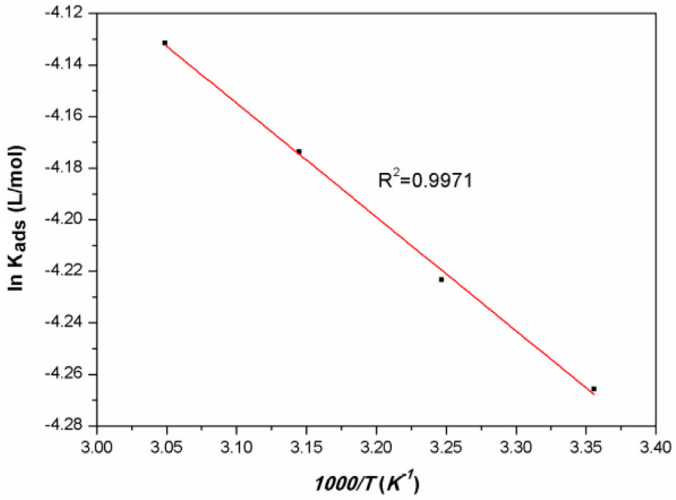

Fig. 10. Plot of $\ln K_{ads}$ *vs.* $1000/T$ for the **MPTM** inhibitor.

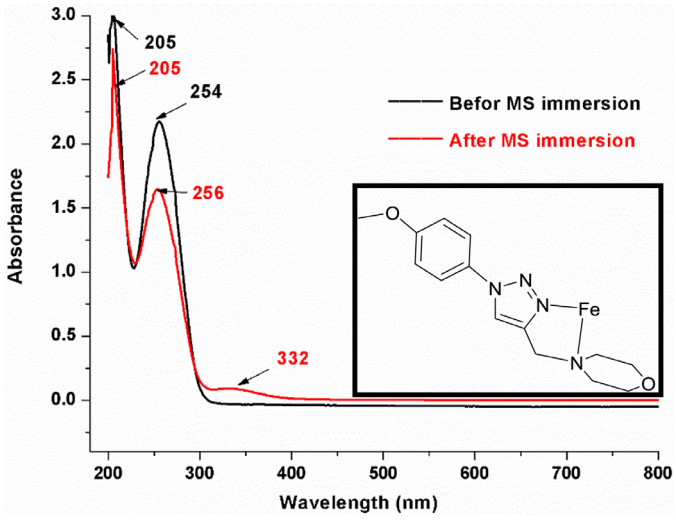

Fig. 11. UV–Vis spectra of 1 M HCl solution with 900 ppm of **MPTM** before and after immersion of the steel sample for 48 h at 298 K. Inset: Possible complex formation between MPTM and the metallic iron on the metallic surface.

3.7. FTIR spectroscopy

FTIR spectroscopic measurements were performed to identify the presence of active groups in the inhibitor molecules (**MPTM**), ensuring the presence of inhibitor film formed on the surface of the MS. Fig. 12 shows the FTIR spectra for the pure and adsorbed **MPTM** on the surface of the MS in 1 M HCl (**A-MPTM**). This figure shows that there are many peaks in the specific spectral ranges of the two samples. Depending on the pure **MPTM** trace, the vibrations of the different bonds such as C-H (sp^3), C=C, C-N, C-O, and =C-H appear at 2930-2802 and 1449, 1610, 1260, 1117 and 1035, and 822 cm^{-1}, respectively. A comparison of the FT-IR spectra before and after the adsorption of **MPTM** on MS show the presence of a strong intensity peak at 3425 cm^{-1} which is related to the presence of the OH group from the water molecule. These observations indicate the formation of a **Fe-MPTM** complex on the surface of the metal, which explains the coordination of the 1,2,3-triazole compound with the iron ions in agreement with the result of UV-Vis test [66]. As a result, the two FTIRspectra indicate that the **MPTM** molecule adsorbed on the surface of the MS forms a protective layer [67].

3.8. Surface Study

To investigate the surface morphology of MS after and before the adsorption of **MPTM**, the SEM and Energy-dispersive X-ray spectroscopy (EDX) analyses were carried out for steel samples in

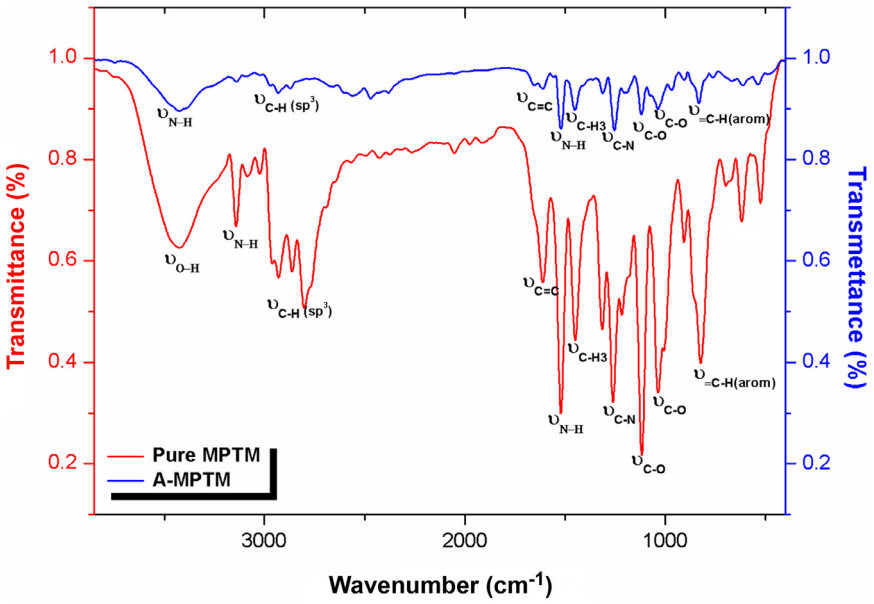

Fig. 12. FTIR spectra of the pure **MPTM** and the its adsorbed phase on the MS surface in 1 M HCl (**A-MPTM**).

acidic solution (Fig. 13). Fig. 13a shows that the surface of the MS sample is very smooth and it does not exhibit any sign of corrosion. However, it appears that the sample of steel without inhibitor (see Fig. 13b) is strongly attacked and one can see more corrosion products and cracks on the surface of the working electrode. In contrast, the significant improvement in the MS surface (Fig. 13c) reflects the high adsorption ability of **MPTM** on the MS surface, suggesting the formation of a protective inhibitor film. The EDX analysis given in Fig. 16 shows that the abraded MS sample (Fig. 13a) reveals the typical peaks of the elements constituting the MS sample. Characteristic peaks of the O and Cl elements containing a corroded surface film of the sample are clearly observed in Fig. 13b. In the same way, the appearance of new nitrogen, carbon, and oxygen peaks in the adsorbed film confirms that the **MPTM** molecule has been strongly adsorbed on the surface of the MS, as shown in Fig. 13c.

3.9. Quantum chemical calculations

Corrosion tests show that the examined compound can effectively protect MS from the corrosion process in acidic medium. Accordingly, quantum chemical calculations and Fukui functions are used to study the interaction between **MPTM** and the iron surfaces and to explain the experimental findings. The optimized structure of **MPTM** was computed using DFT calculations at the B3LYP/6-31G (d, p) level (Fig. 14a). It can be observed in Fig. 14b that the HOMO orbital is more centrated on the morpholine ring rather than on the triazole or phenyl rings, indicating that the morpholine ring is the more important segment that can donate an electron to the metal atoms. However, the LUMO orbital is dominantly concentrated on the triazole and phenyl rings (Fig. 14c), suggesting that these motifs have stronger electron-accepting ability. Moreover, molecular electrostatic potential (MEP) maps provide additional insights on the responsible sites for the adsorption process (Fig. 14 d). This map shows the region of a molecule in which the electron density is more located than in the other ones; the blue areas represent the region of the most positive MEP whereas the red parts correspond to the zones of the most negative MEP. The results reflect that the oxygen atoms and the nitrogen atom of triazole ring have high negative charge density, indicating the sites with high ability to interact with the metal surface.

Table 9
Fukui indices calculated for the **MTPM** molecule at the B3LYP/6-31G (b,p) level

Atom	Number	f_k^+	f_k^-	Df_k
C	1	**0.1097**	0.0084	0.1012
C	2	0.0413	0.0153	0.0260
N	4	0.0841	0.0417	0.0423
N	5	**0.1036**	0.0424	0.0612
N	6	0.0095	0.0078	0.0017
C	7	-0.0089	-0.0236	0.0147
C	10	-0.0049	-0.0213	0.0164
C	11	-0.0010	-0.0219	0.0208
C	12	-0.0036	-0.0105	0.0069
C	15	-0.0009	-0.0074	0.0065
N	22	-0.0060	**0.1966**	-0.2026
O	23	0.0064	0.0323	-0.0258
C	24	0.0599	**0.0588**	0.0010
C	25	0.0321	0.0049	0.0272
C	26	0.0802	0.0177	0.0625
C	27	0.0370	0.0427	-0.0056
C	29	0.0072	0.0338	-0.0265
C	31	**0.1199**	0.0477	0.0721
O	34	0.0276	**0.0725**	-0.0448
C	35	-0.0124	-0.0137	0.0013

Fukui indices are a powerful way to identify the most nucleophilic and electrophilic sites in a molecule. The condensed Fukui functions for the nucleophilic (f_k^+) and the electrophilic attacks (f_k^-) for **MPTM** are calculated and they are summarized in Table 9. The atoms with a higher f_k^+ are more probable to donate an electron to the metal surface, whereas those with a higher $f_k^-$are more probable to accept an electron from the iron surface [68,69]. The analysis of the Fukui indices shows that **MPTM** has several active donor-acceptors, which can promote the adsorption of this molecule on the surface of the metal. Overall, these results indicate that the C(31), N(5) and C(1) sites have high values of f_k^+, while the high values of f_k^- functions are positioned on the N(22), O(34) and C(24) atoms (Table 9). The dual descriptors derivate from Fukui functions are shown in Fig. 15, indicating electron acceptor sites (in purple) and electron donor sites (in blue). These findings are in good agreement with the distribution of the HOMO and LUMO orbitals, and they prove the important sites for the adsorption of **MPTM** molecule on the MS surface.

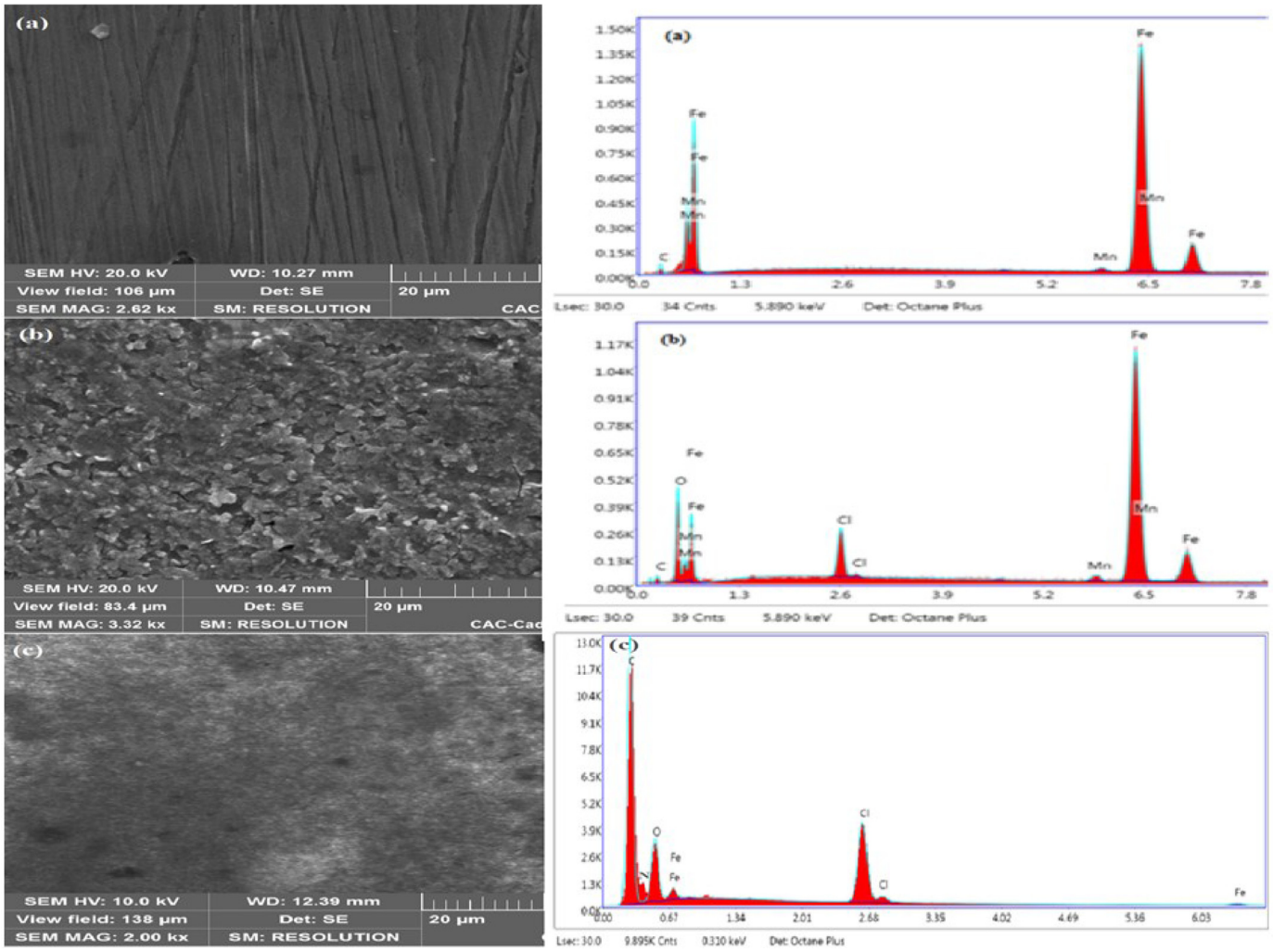

Fig. 13. SEM images and EDX spectra of MS (a) alone, (b) corroded after 24 h of immersion time in a 1 M HCl solution and (c) after immersion with 900 ppm **MPTM** at 298 K.

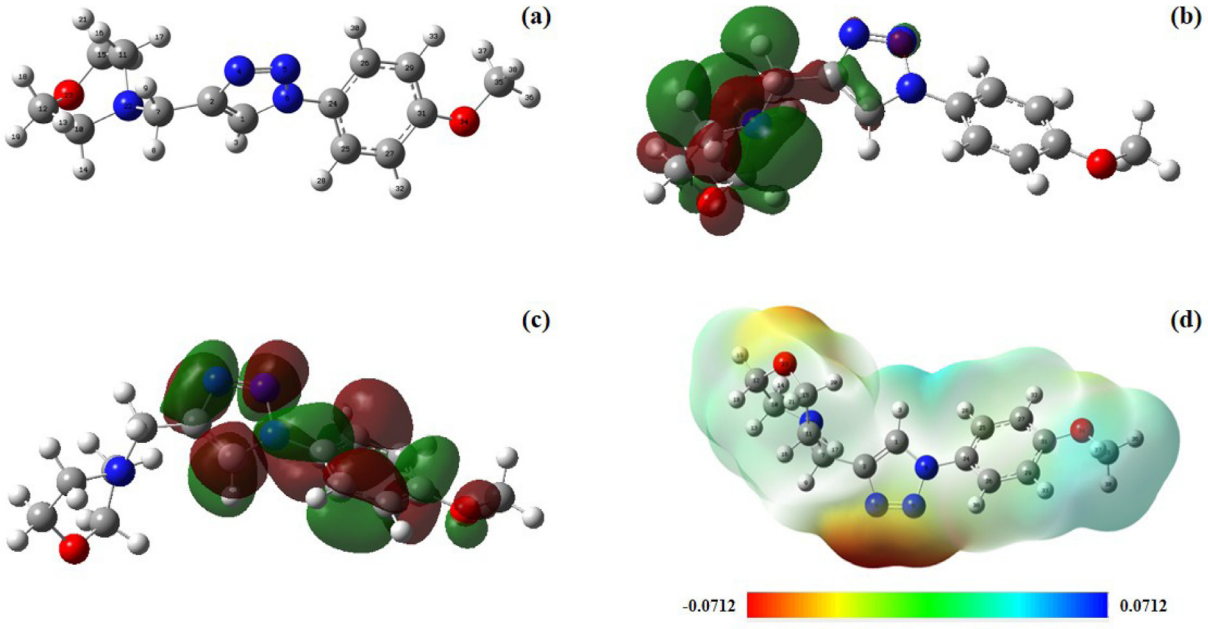

Fig. 14. Optimized structures of **MPTM** (a), HOMO (b), LUMO (c) and MEP (d) by using DFT calculations at the B3LYP/6-31G(d, p) level.

Table 10
Comparison of **MPTM** inhibitor with previously reported inhibitors containing the 1,2,3-triazole unit in 1 M HCl.

Entry	Name	Structure	C (M)	*IE*(%)[a]	Ref
1	4-[1-(4-Methoxy-phenyl)-1*H*-[1,2,3]triazol-4-ylmethyl]-morpholine (**MPTM**)	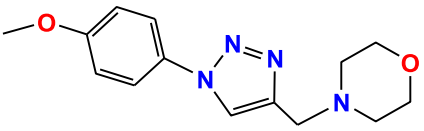	1	94	**This work**
2	[3-(4-Phenyl-[1.2.3]triazol-1-yl)-propyl]-phosphonic acid diethyl ester ($\mathbf{P_1}$)	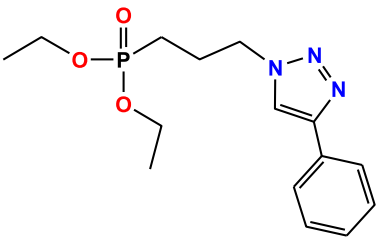	1	90.7	[21]
3	{3-[4-(4-Dimethylamino-phenyl)-[1.2.3]triazol-1-yl]-propyl}-phosphonic acid diethyl ester ($\mathbf{P_2}$)	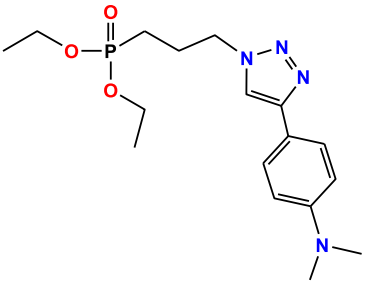	1	93.6	[21]
4	2-{[1-(4-Fluorobenzyl)-1*H*-1,2,3-triazol-4-yl]methylthio}-1*H*-benzimidazole ($\mathbf{P_3}$)	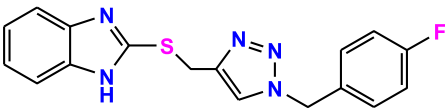	1	96	[71]
5	1-[(1-Benzyl-1*H*-1,2,3-triazol-4-yl)methyl]-2-[(1-benzyl-1*H*-1,2,3-triazol-4-yl)methylthio]-1*H*-benzimidazole ($\mathbf{P_4}$)	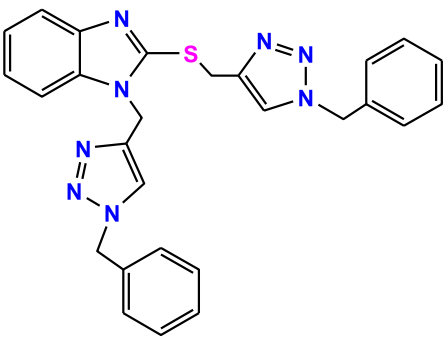	1	98	[71]
6	1-*p*-Tolyl-1*H*-1,2,3-triazol-4-yl) methanol ($\mathbf{P_5}$)	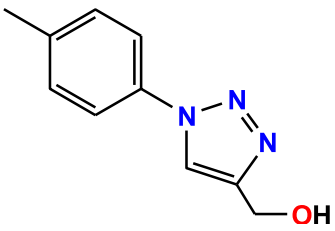	1	83.1	[72]

(*continued on next page*)

Table 10 (*continued*)

Entry	Name	Structure	C (M)	*IE(%)*[a]	Ref
7	1-(4-Iodobenzyl)-4-phenoxymethyl-1*H*-1,2,3-triazole (**P_6**)	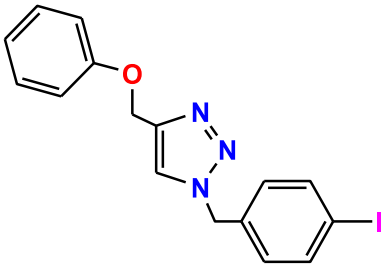	1	96.1	[73]

[a] Inhibition efficiency measured at 298 K.

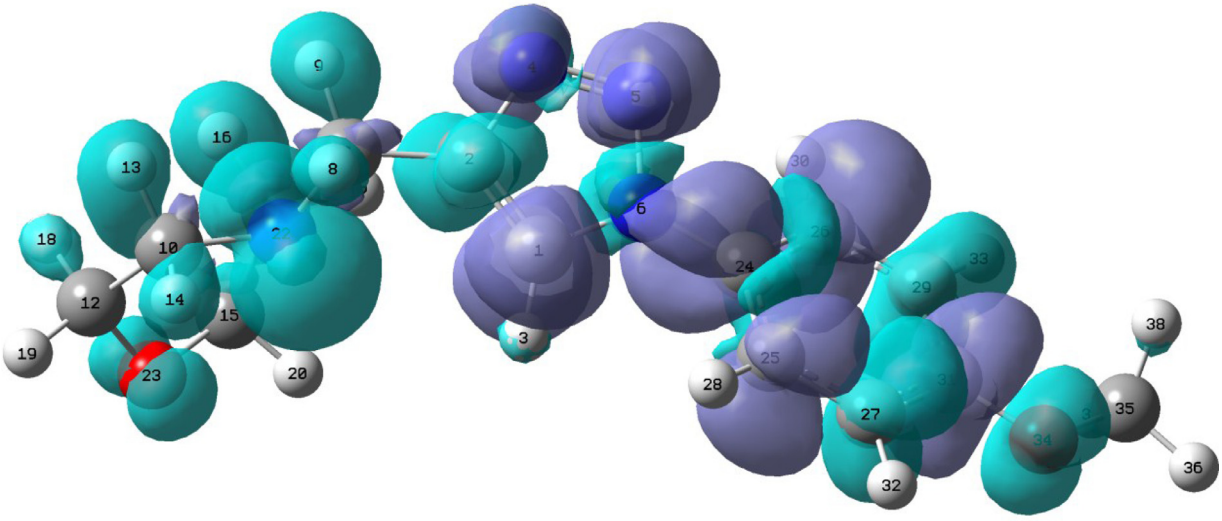

Fig. 15. Dual descriptor Fukui functions for the **MTPM** molecule at the B3LYP/6-31G (b,p) level.

3.10. Comparison of MPTM with other inhibitors

1,2,3-triazole derivatives have been studied for their capacity to inhibit corrosion behavior in aggressive media [70]. Table 10 trates the use of 1,4-disubstituted 1,2,3-triazole derivatives as corrosion inhibitors for MS under the same conditions. As shown in Table 10, **MPTM** was found to be similar to the **P_1** and **P_2** molecules, but better than the **P_5** one, while the presence of more strongly electronegative atoms (F and I) at **P_3** and **P_6** or a greater number of heteroatoms (**P_4**) in inhibitors structures makes them good candidates as new efficient triazolic corrosion inhibitors.

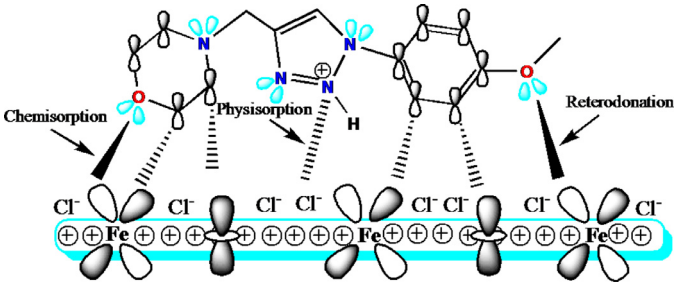

Fig. 16. Proposed adsorption mechanism of **MPTM** on the surface of MS in 1 M HCl.

3.11. Corrosion inhibition mechanism

Based on the electrochemical part, the surface examination and the DFT calculations, a mechanism for the adsorption of the **MPTM** inhibitor on the surface of mild steel is proposed that is shown in Fig. 16. According to our thermodynamic results, the adsorption behavior of the **MPTM** inhibitor on the MS surface in the hydrochloric medium includes both physical and chemical adsorptions (Fig. 16). In the corrosive solution, MS undergoes a fast oxidation, which makes the metal surface positively charged, attracting negatively charged counterions such as chloride anions. On the other hand, the triazole group of the **MPTM** molecule is protonated, a feature that promotes electrostatic interactions with the Cl^- anions adsorbed on the surface of the MS (physisorption). In parallel, the chemisorption takes place by the donation of a single electron pair of the heteroatoms (O, N) and π-delocalized electrons from the benzene ring to the vacant *3d*-orbitals of Fe [74]. The high reactivity of **MPTM**, due to the presence of the O-morpholine group, allows additional chemisorption. In addition, the π donation of the phenyl ring electrons to the vacant *3d* Fe orbitals and simultaneously its vacant anti-bonding π orbital offers to accept electrons from the filled metal orbitals causing the back-bonding phenomenon, which provides the additional potential of the **MPTM** inhibitor to interact with the mild steel [75].

4. Conclusion

A new 1,2,3-triazole compound bearing morpholine moiety namely, 4-[1-(4-methoxyphenyl)-1*H*-[1,2,3]triazol-4-ylmethyl]-morpholine (**MPTM**), was synthesized under click chemistry regime in an excellent yield. The obtained 1,2,3-triazole derivative was characterized using different techniques such as ^{1}H NMR, ^{13}C NMR, HRMS, and FTIR spectroscopy. This synthetic triazole showed promising results as an excellent corrosion inhibitor at ppm traces (94% was achieved at 900 ppm concentration), and their adsorption on the steel surface occurred through both physi- and chemisorption mechanisms following the Langmuir adsorption isotherm. SEM, EDX and FT-IR analysis were used to confirm the formation of a protective film of the **MPTM** on the steel surface. Moreover, our theoretical study provided better insights to identify the responsible sites for the adsorption of **MPTM** on the MS surface and all the outcomes support the experimental findings.

Declaration of Competing Interest

The authors declare that they have no known competing financial interests or personal relationships that could have appeared to influence the work reported in this paper.

Acknowledgements

The Spanish Ministerio de Ciencia e Innovacion (MCINN) (Projects CTQ2016-75068P) is gratefully acknowledged for generous support.

Supplementary materials

Supplementary material associated with this article can be found, in the online version, at doi:10.1016/j.molstruc.2021.129895.

References

[1] G. Li, J.A. Field, C. Zeng, C.L. Madeira, C.H. Nguyen, K.V. Jog, D. Speed, R. Sierra-Alvarez, Diazole and triazole inhibition of nitrification process in return activated sludge, Chemosphere 241 (2020) 124993.
[2] S. Kumar Avula, A. Khan, S. Ahsan Halim, Z. Al-Abri, M.U. Anwar, A. Al-Rawahi, R. Csuk, A. Al-Harrasi, Synthesis of novel (R)-4-fluorophenyl-1*H*-1,2,3-triazoles: A new class of α-glucosidase inhibitors, Bioorg. Chem. 91 (2019) 103182.
[3] W.Q. Fan, A.R. Katritzky, in: A.R. Katritzky, C.W. Rees, E.F. Scriven (Eds.), 1,2,3-Triazoles In Heterocyclic Chemistry II, 4, Pergamon Press, Oxford, 1996, pp. 1–126. Eds.
[4] S.A. Haddadi, E. Alibakhshi, G. Bahlakeh, B. Ramezanzadeh, M. Mahdavian, A detailed atomic level computational and electrochemical exploration of the Juglansregia green fruit shell extract as a sustainable and highly efficient green corrosion inhibitor for mild steel in 3.5 wt% NaCl solution, J. Mol. Liq. 284 (2019) 682–699.
[5] M. Tisza, I. Czinege, Comparative study of the application of steels and aluminum in lightweight production of automotive parts, Int. J. Lightweight. Mater. Manuf. 1 (4) (2018) 229–238.
[6] A. Boutouil, M.R. Laamari, I. Elazhary, H. Anane, A. BenTama, S.E. Stiriba, A new insight into corrosion inhibition process of mild steel in sulfuric acid medium: a combined experimental and theoretical study, Anti-Corros. Method. m. 66 (2019) 835–852.
[7] C. Verma, H. Lgaz, D.K. Verma, E.E. Ebenso, I. Bahadur, M.A. Quraishi, Molecular dynamics and Monte Carlo simulations as powerful tools for study of interfacial adsorption behavior of corrosion inhibitors in aqueous phase: A review, J. Mole. Liq. 260 (2018) 99–120.
[8] C. Verma, M.A. Quraishi, E.E. Ebenso, I. Bahadur, A Green and Sustainable Approach for Mild Steel Acidic Corrosion Inhibition Using Leaves Extract: Experimental and DFT Studies, J. Bio. Tribo. Corros. 4 (2018) 33.
[9] A. Dehghani, G. Bahlakeh, B. Ramezanzadeh, A detailed electrochemical/theoretical exploration of the aqueous Chinese gooseberry fruit shell extract as a green and cheap corrosion inhibitor for mild steel in acidic solution, J. Mol. Liq. 282 (2019) 366–384.
[10] I. Elazhary, A. Boutouil, H. Ben El Ayouchia, M.R. Laamari, M.El Haddad, H. Anane, S.E. Stiriba, Anti-Corrosive Properties of (1-benzyl-1*H*-1,2,3-triazol-4-yl) Methanol on Mild Steel Corrosion in Hydrochloric Acid Solution: Experimental and Theoretical Evidences, Prot. Met. Phys. Chem. Surf. 55 (1) (2019) 166–178.
[11] N. Shet, R. Nazareth, P.A. Suchetan, Corrosion Inhibition of 316 Stainless Steel in 2M HCl by 4-{[4-(dimethylamino)benzylidene]amino}-5-methyl-4*H*-1,2,4-triazole-3-thiol, Chem. Data. Collect. 20 (2019) 100209.
[12] R. Hasanov, S. Bilge, S. Bilgiç, G. Gece, Z. Kılıç, Experimental and theoretical calculations on corrosion inhibition of steel in 1M H_2SO_4 by crown type polyethers, Corr. Sci. 52 (3) (2010) 984–990.
[13] A. Chetouani, A. Aouniti, B. Hammouti, N. Benchat, T. Benhadda, S. Kertit, Corrosion inhibitors for iron in hydrochloride acid solution by newly synthesized pyridazine derivatives, Corr. Sci. 45 (8) (2003) 1675–1684.
[14] M. Abdallah, H.E. Meghed, M. Sobhi, Inhibiting effect of Ni^{2+} cation^{+3}-methyl pyrazolone as a corrosion inhibitor for carbon steel in sulfuric acid solution, Mater. Chem. Phys. 118 (1) (2009) 111–117.
[15] X. Cheng, H. Ma, S. Chen, R. Yu, X. Chen, Z. Yao, Corrosion of stainless steels in acid solutions with organic sulfur-containing compounds, Corr. Sci. 41 (2) (1998) 321–333.
[16] A. Boutouil, I. Elazhary, M.R. Laamari, H. Ben El Ayouchia, H. Anane, M.El Haddad, S.E. Stiriba, An exploration of corrosion inhibition of mild steel in sulphuric acid solution through experimental study and Monte Carlo simulations, J. Adhes. Sci. Techno. 34 (2020) 549–578.
[17] H.C. Kolb, M.G. Finn, K.B. Sharpless, Diverse chemical function from a few good reactions, Angew, Chem. Int. Ed. 40 (11) (2001) 2004–2021.
[18] L. Bahsis, H. Ben El Ayouchia, H. Anane, S. Triki, M. Julve, S.E. Stiriba, Copper(II)-dipicolinate-mediated clickable azide alkyne cycloaddition in water as solvent, J. Coord. Chem. 71 (2018) 633–643.
[19] N. Aflak, H. Ben El Ayouchia, L. Bahsis, E.M. El Mouchtari, M. Julve, S. Rafqah, H. Anane, S.E. Stiriba, Sustainable Construction of Heterocyclic 1,2,3-Triazoles by Strict Click [3+2] Cycloaddition Reactions Between Azides and Alkynes on Copper/Carbon in Water, Front. Chem. 7 (2019) 81.
[20] A. Oubella, M.Y. AitItto, A. Auhmani, A. Riahi, A. Robert, J.C. Daran, H. Morjanid, C.A. Parish, M. Esseffar, Diastereoselective synthesis and cytotoxic evaluation of new isoxazoles and pyrazoles with monoterpenic skeleton, J. Mol. Struct. 1198 (2019) 126924.
[21] M. Hrimla, L. Bahsis, A. Boutouil, M.R. Laamari, M. Julve, S.E. Stiriba, A combined computational and experimental study on the mild steel corrosion inhibition in hydrochloric acid by new multifunctional phosphonic acid containing 1,2,3-triazoles, J. Adhes. Sci. Techno. (2020) 1–33.
[22] M.M. Solomon, S.A. Umoren, M.A. Quraishi, M. Salman, Myristic acid based imidazoline derivative as effective corrosion inhibitor for steel in 15% HCl medium, J. Colloid. Interf. Sci. 551 (2019) 47–60.
[23] O. Dagdag, Z. Safi, N. Wazzan, H. Erramli, L. Guo, A.M. Mkadmh, C. Verma, E.E. Ebenso, L.El Gana, A.El Harfi, Highly functionalized epoxy macromolecule as an anti-corrosive material for carbon steel: Computational (DFT, MDS), surface (SEM-EDS) and electrochemical (OCP, PDP, EIS) studies, J. Mol. Liq. 302 (2020) 112535.
[24] Y. Achour, M. Khouili, H. Abderrafia, S. Melliani, M.R. Laamari, M.El Haddad, DFT Investigations and Experimental Studies for Competitive and Adsorptive Removal of Two Cationic Dyes onto an Eco-friendly Material from Aqueous Media, Int. J. Environ. Res. 12 (2018) 789–802.
[25] I. Wilkening, G. del. Signore, C.P.R. Hackenberger, Synthesis of phosphonamidate peptides by Staudinger reactions of silylated phosphinic acids and esters, Chem. Commun. 47 (1) (2011) 349–351.
[26] L. Bahsis, H. Ben El Ayouchia, H. Anane, K. Benhamou, H. Kaddami, M. Julve, S.E. Stiriba, Cellulosecopper as bio-supported recyclable catalyst for the clickable azide-alkyne [3 + 2] cycloaddition reaction in water, Int. J. Biol. Macromol. 119 (2018) 849–856.
[27] A. Boutouil, M. Hrimla, M.R. Laamari, I. Elazhary, H. Ben El Ayouchia, M.El Haddad, H. Anane, S.E. Stiriba, Understanding the Corrosion Inhibition Mechanism of Mild Steel in Hydrochloric Acide by a Triazole Derivative: A Combined Experimental and Theoretical Approach, Prot. Met. Phys. Chem. Surf. 55 (2019) 973–985.
[28] M.J. Frisch, G.W. Trucks, H.B. Schlegel, G.E. Scuseria, M.A. Robb, J.R. Cheeseman, G. Scalmani, V. Barone, B. Mennucci, G.A. Petersson, H. Nakatsuji, M. Caricato, X. Li, H.P. Hratchian, A.F. Izmaylov, J. Bloino, G. Zheng, J.L. Sonnenberg, M. Hada, M. Ehara, K. Toyota, R. Fukuda, J. Hasegawa, M. Ishida, T. Nakajima, Y. Honda, O. Kitao, H. Nakai, T. Vreven, J.A. Montgomery, J.E. Peralta Jr, F. Ogliaro, M. Bearpark, J.J. Heyd, E. Brothers, K.N. Kudin, V.N. Staroverov, R. Kobayashi, J. Normand, J. Raghavachari, A. Rendell, J.C. Burant, S.S. Iyengar, J. Tomasi, M. Cossi, N. Rega, J.M. Millam, M. Klene, J.E. Knox, J.B. Cross, V. Bakken, C. Adamo, J. Jaramillo, R. Gomperts, R.E. Stratmann, O. Yazyev, A.J. Austin, R. Cammi, C. Pomelli, J.W. Ochterski, R.L. Martin, K. Morokuma, V.G. Zakrzewski, G.A. Voth, P. Salvador, J.J. Dannenberg, S. Dapprich, A.D. Daniels, O. Farkas, J.B. Foresman, J.V. Ortiz, J. Cioslowski, D.J. Fox, Gaussian 09, Gaussian. Inc, Wallingford. C.T., 2009.
[29] R.G. Parr, W. Yang, Density Functional Approach to the Frontier-Electron Theory of Chemical Reactivity, J. Am. Chem. Soc. 106 (1984) 4049–4050.
[30] T. Lu, F.W. Chen, Multiwfn: a multifunctional wave function analyzer, J. Comput. Chem. 33 (2012) 580–592.
[31] M.G. Sethuraman, V. Aishwarya, C. Kamal, T.Jebakumar Immanuel Edison, Studies on Ervatinine – The anticorrosive phyto constituent of Ervatamiacoronaria, Arab. J. Chem. 10 (2017) S522–S530.
[32] D.K. Yadav, M.A. Quraishi, Electrochemical investigation of Substituted Pyranopyrazoles Adsorption on Mild Steel in Acid Solution, Ind. Eng. Chem. Res. 51 (24) (2012) 8194–8210.

[33] L. Jiang, Y. Qiang, Z. Lei, J. Wang, Z. Qin, B. Xiang, Excellent corrosion inhibition performance of novel quinoline derivatives on mild steel in HCl media: Experimental and computational investigations, J. Mol. Liq. 255 (2018) 53–63.
[34] X. Zheng, S. Zhang, W. Li, L. Yin, J. He, J. Wu, Investigation of 1-butyl-3-methyl-1*H*-benzimidazolium iodide as inhibitor for mild steel in sulfuric acid solution, Corros. Sci. 80 (2014) 383–392.
[35] S. Issaadi, T. Douadi, A. Zouaoui, S. Chafaa, M.A. Khan, G. Bouet, Novel thiophene symmetrical Schiff base compounds as corrosion inhibitor for mild steel in acidic media, Corros. Sci. 53 (4) (2011) 1484–1488.
[36] A. Döner, R. Solmaz, M. Özcan, G. Kardaş, Experimental and theoretical studies of thiazoles as corrosion inhibitors for mild steel in sulphuric acid solution, Corros. Sci. 53 (9) (2011) 2902–2913.
[37] H. Hamani, T. Douadi, M. Al-Noaimi, S. Issaadi, D. Daoud, S. Chafaa, Electrochemical and quantum chemical studies of some azomethine compounds as corrosion inhibitors for mild steel in 1 M hydrochloric acid, Corros. Sci. 88 (2014) 234–245.
[38] F. Bentiss, M. Bouanis, B. Mernari, M. Traisnel, H. Vezi, M. Lagrenée, Understanding the adsorption of 4-*H*-1,2,4-triazole derivatives on mild steel surface in molar hydrochloric acid, Appl. Surf. Sci. 253 (7) (2007) 3696–3704.
[39] A.El Bribri, M. Tabyaoui, B. Tabyaou, H.El Attari, F. Bentiss, The use of Euphorbia falcata extract as eco-friendly corrosion inhibitor of carbon steel in hydrochloric acid solution, Mater. Chem. Phys. 141 (1) (2013) 240–247.
[40] C. Verma, A.A. Sorour, E.E. Ebenso, M.A. Quraishi, Inhibition performance of three naphthyridine derivatives for mild steel corrosion in 1 M HCl: Computation and experimental analyses, Results. Phys. 10 (2018) 504–511.
[41] M.R. Laamari, J. Benzakour, F. Berrekhis, A. Abouelfida, A. Derja, D. Villemin, Corrosion inhibition of carbon steel in hydrochloric acid 0.5M by hexa methylene diaminetetramethyl-phosphonic acid, Arab. J. Chem. 4 (3) (2011) 271–277.
[42] C.M. Fernandes, L.X. Alvarez, N.E. dos Santos, A.C. Maldonado Barrios, E.A.E.A. Ponzio, Green synthesis of 1-benzyl-4-phenyl-1*H*-1,2,3-triazole, its application as corrosion inhibitor for mild steel in acidic medium and new approach of classical electrochemical analyses, Corros. Sci. 194 (2019) 185–194.
[43] D. Wang, B. Xiang, Y. Liang, S. Song, C. Liu, Corrosion control of copper in 3.5wt% NaCl Solution by Domperidone: Experimental and Theoretical Study, Corros. Sci. 85 (2014) 77–86.
[44] Y. Qiang, S. Zhang, S. Xu, W. Li, Experimental and theoretical studies on the corrosion inhibition of copper by two indazole derivatives in 3.0% NaCl solution, J. Colloid. Interf. Sci. 472 (2016) 52–59.
[45] I. Elazhary, A. Boutouil, H. Ben El Ayouchia, M.R. Laamari, M.El Haddad, H. Anane, S.E. Stiriba, Anti-Corrosive Properties of (1-benzyl-1*H*-1,2,3-triazol-4-yl) Methanol on Mild Steel Corrosion in Hydrochloric Acid Solution: Experimental and Theoretical Evidences, Prot. Met. Phys. Chem. Surf. 55 (1) (2019) 166–178.
[46] M. Talebian, K. Raeissi, M. Atapour, B.M. Fernández-Pérez, Z. Salarvand, S. Meghdadi, M. Amirnasr, R.M. Souto, Inhibitive effect of sodium (E)-4-(4-nitrobenzylideneamino)benzoate on the corrosion of some metals in sodium chloride solution, Appl. Surf. Sci. 447 (2018) 852–865.
[47] R. Solmaz, G. Kardaş, M. Çulha, B. Yazıcı, M. Erbil, Investigation of adsorption and inhibitive effect of 2-mercaptothiazoline on corrosion of mild steel in hydrochloric acid media, Electrochim.Acta 53 (20) (2008) 5941–5952.
[48] M. Tourabi, K. Nohair, M. Traisnel, C. Jama, F. Bentiss, Electrochemical and XPS studies of the corrosion inhibition of carbon steel in hydrochloric acid pickling solutions by 3,5-bis(2-thienylmethyl)-4-amino-1,2,4-triazole, Corros. Sci. 75 (2013) 123–133.
[49] M.A.Quraishi Sudheer, Electrochemical and theoretical investigation of triazole derivatives on corrosion inhibition behavior of copper in hydrochloric acid medium, Corros. Sci. 70 (2013) 161–169.
[50] R.N. Vyas, K. Li, B. Wang, Modifying Randles Circuit for Analysis of Polyoxometalate Layer-by-Layer Films, J. Phys. Chem. B. 114 (48) (2010) 15818–15824.
[51] T.H. Silva, V. Garcia-Morales, C. Moura, J.A. Manzanares, F. Silva, Electrochemical Impedance Spectroscopy of Polyelectrolyte Multilayer Modified Gold Electrodes: Influence of Supporting Electrolyte and Temperature, Langmuir. 21 (16) (2005) 7461–7467.
[52] L. Jiang, Y. Qiang, Z. Lei, J. Wang, Z. Qin, B. Xiang, Excellent corrosion inhibition performance of novel quinoline derivatives on mild steel in HCl media: Experimental and computational investigations, J. Mol. Liq. 255 (2018) 53–63.
[53] K.F. Al-Azawi, I.M. Mohammed, S.B. Al-Baghdadi, T.A. Salman, H.A. Issa, A.A. Al-Amiery, S.G. Gaaz, A.A.H. Kadhum, Experimental and quantum chemical simulations on the corrosion inhibition of mild steel by 3-((5-(3,5-dinitrophenyl)-1,3,4-thiadiazol-2-yl)imino)indolin-2-one, Res. Phys. 9 (2018) 278–283.
[54] M.R. Laamari, J. Benzakour, F. Berrekhis, A. Derja, D. Villemin, Adsorption and corrosion inhibition of carbon steel in hydrochloric acid medium by hexamethylene diaminetetra(methylene phosphonic acid), Arab. J. Chem. 9 (2016) S245–S251.
[55] H.H. Zhang, Y. Chen, Z. Zhang, Comparative studies of two benzaldehyde thiosemicarbazone derivatives as corrosion inhibitors for mild steel in 1 M HCl, Res. Phys. 11 (2018) 554–563.
[56] L. Zhou, Y.L. Lv, Y.X. Hu, J.H. Zhao, X. Xia, X. Li, Experimental and theoretical investigations of 1,3,5-tris(4-aminophenoxy)benzene as an effective corrosion inhibitor for mild steel in 1 M HCl, J. Mol. Liq. 249 (2018) 179–187.
[57] M. Rbaa, F. Benhiba, I.B. Obot, H. Oudda, I. Warad, B. Lakhrissi, A. Zarrouk, Two new 8-hydroxyquinoline derivatives as an efficient corrosion inhibitors for mild steel in hydrochloric acid: Synthesis, electrochemical, surface morphological, UV–visible and theoretical studies, J. Mol. Liqu. 276 (2018) 120–133.
[58] P. Rugmini Ammal, M. Prajila, A. Joseph, Physicochemical studies on the inhibitive properties of a 1,2,4-triazole Schiff's base, HMATD, on the corrosion of mild steel in hydrochloric acid, Egypt. J. Petrol. 27 (3) (2017) 307–317.
[59] I.B. Obot, E.E. Ebenso, I.A. Akpan, Z.M. Gasem, A.S. Afolabi, Thermodynamic and Density Functional Theory Investigation of Sulphathiazole as Green Corrosion Inhibitor at Mild Steel/Hydrochloric Acid Interface, Int. J. Electrochem. Sci. 7 (2012) 1978–1996.
[60] T. Brindha, K. Parimalagandhi, J. Mallika, Thermodynamic and Electrochemical Analysis of Synergistic Corrosion Inhibition Performance of Natural Polysaccharides with Metal Halides on Mild Steel in Hydrochloric Acid Solution, J. Bio. Tribo. Corros. 6 (1) (2019) 3.
[61] A.S. Yusuff, Adsorption of hexavalent chromium from aqueous solution by Leucaenaleucocephalaseed pod activated carbon: equilibrium, kinetic and thermodynamic studies, Arab. J. Basic. Appl. Sci. (2019) 1–14.
[62] M. Abdallah, M. El-Naggar, Cu^{+2} cation^{+3},5-dimethyl pyrazole mixture as a corrosion inhibitor for carbon steel in sulfuric acid solution, Mater. Chem. Phys. 71 (3) (2001) 291–298.
[63] I.B Obot, N.O. Obi-Egbedi, A.O. Eseola, Anticorrosion Potential of 2-Mesityl-1*H*-imidazo[4,5-f][1,10]phenanthroline on Mild Steel in Sulfuric Acid Solution: Experimental and Theoretical Study, Industrial & Engineering Chemistry Research 50 (4) (2011) 2098–2110.
[64] Y. Abboud, A. Abourriche, T. Saffaj, M. Berrada, M. Charrouf, A. Bennamara, N. Al Himidi, H. Hannache, 2,3-Quinoxalinedione as a novel corrosion inhibitor for mild steel in 1M HCl, Mater. Chem. Phys. 105 (1) (2007) 1–5.
[65] Z. Rouifi, F. Benhiba, M.E. Faydy, T. Laabiassi, H. About, H. Oudda, I. Warad, A. Guenbour, B. Lakhrissi, A. Zarrouk, Performance and computational studies of new soluble triazole as corrosion inhibitor for carbon steel in HCl, Chem. Data. Collect. 22 (2019) 100242.
[66] I.M. Chung, K. Kalaiselvi, A. Sasireka, S.H. Kim, M. Prabakaran, Anticorrosive property of Spiraea Cantoniensisis extract as an eco-friendly inhibitor on mild steel surface in acid medium, J. Disper. Sci. Technol. 40 (9) (2018) 1326–1337.
[67] M. Prabakaran, S.H. Kim, N. Mugila, V. Hemapriya, K. Parameswari, S. Chitra, I.M. Chung, Aster koraiensis as nontoxic corrosion inhibitor for mild steel in sulfuric acid, J. Ind. Eng. Chem. 52 (2017) 235–242.
[68] A.Y. Musa, A.H. Kadhum, A.B. Mohamad, A.B. Rahoma, H. Mesmari, Electrochemical and quantum chemical calculations on 4,4-dimethyloxazolidine-2-thione asinhibitor for mild steel corrosion in hydrochloric acid, J. Mol. Struct. 969 (2010) 233–237.
[69] I. Lukovits, E. Kálmán, F. Zucchi, Corrosion inhibitors - Correlation between electronic structure and efficiency, Corros 57 (2001) 3–8.
[70] M. Faisal, A. Saeed, D. Shahzad, N. Abbas, F. Ali Larik, P. Ali Channar, T. Abdul Fattah, D. Muhammad Khan, S. Aaliya Shehzadi, General properties and comparison of the corrosion inhibition efficiencies of the triazole derivatives for mild steel, Corros Rev 0 (0) (2018).
[71] G. Negrón-Silva, D. Cruz-Gonzalez, R. González-Olvera, L. Lomas-Romero, A. Gutiérrez-Carrillo, M. Palomar-Pardavé, M.A. Romero-Romo, R. Santillan, J. Uruchurtu, One-Pot Three-Component Synthesis of New Mono- and Bis-1,2,3-triazole Derivatives of 2-Benzimidazolethiol with a Promising Inhibitory Activity against Acidic Corrosion of Steel, Synthesis 46 (09) (2014) 1217–1223.
[72] A Boutouil, M.R. Laamari, I. Elazhary, L. Bahsis, H. Anane, S.E. Stiriba, Towards a deeper understanding of the inhibition mechanism of a new 1,2,3-triazole derivative for mild steel corrosion in the hydrochloric acid solution using coupled experimental and theoretical methods, Mater. Chem. Phys. 241 (2020) 122420.
[73] A. Espinoza-Vázquez, F.J. Rodríguez-Gómez, R. González-Olvera, D. Angeles-Beltrán, D. Mendoza-Espinosa, G.E. Negrón-Silva, Electrochemical assessment of phenol and triazoles derived from phenol (BPT) on API 5L X52 steel immersed in 1 M HCl, RSC. Adv. 6 (77) (2016) 72885–72896.
[74] K. Wan, P. Feng, B. Hou, Y. Li, Enhanced corrosion inhibition properties of carboxymethy lhydroxypropyl chitosan for mild steel in 1.0 M HCl solution, RSC. Adv. 6 (81) (2016) 77515–77524.
[75] A. Singh, K.R. Ansari, X. Xu, Z. Sun, A. Kumar, Y. Lin, An impending inhibitor useful for the oil and gas production industry: Weight loss, electrochemical, surface and quantum chemical calculation, Sci. Rep. 7 (1) (2017) 14904.